Growth, structural, morphological, opto-electrical and first-principle investigations of ZnMgS thin films

Published: 16 July 2022

Volume 33, pages 18798–18806, (2022) Cite this article

Journal of Materials Science: Materials in Electronics

Aims and scope

Submit manuscript

Avinash S. Dive, Jitendra S. Kounsalye & Ramphal Sharma

Abstract

Here, we report the chemical synthesis of $Zn_{0.7}Mg_{0.3}S$ columnar nanorods onto a commercial glass slide. The synthesized films were used for further studies. Structural, morphological, optical, and electrical properties were analyzed via X-ray diffraction, FE-SEM, TEM, UV–Vis spectroscopy, and two-probe I–V characteristics, respectively. A stable hexagonal structure with the nanocrystalline size of the ZnMgS material has been confirmed from X-ray and TEM analysis and also structural parameters were determined. FE-SEM micrographs show the uniformity of the grown nanorods on the surface of the film; combined EDX spectra display the presence of Zn, Mg, and S. UV–Vis absorption spectra show a prominent peak at ~ 310 nm which confirms the blue emission spectra. The semiconducting nature of synthesized ZnMgS films was confirmed by the electrical study and the

photosensing ability was examined. Finally, ZnMgS is a direct bandgap semiconductor which is confirmed from first-principle calculations.

1 Introduction

Recently, many reports are available on optical technologies and material modifications for semiconductors. Some of the semiconducting materials are promising candidates for transistors, modern-day's electronics [1], light-emitting diode (LED) [2], photosensors, and low-cost solar cells. With the increase in temperature, the electrical conductivity of the semiconducting material increases substantially which is the exact opposite behavior of the metals. For many decades, researchers and industrialists are focusing on the development of a photoelectronic device or different wavelength photodetectors from separate photosensitive and appropriate bandgap semiconductors [3, 4]. Including the various excellent properties of semiconducting materials, some nanostructures and shapes like 1-dimensional (1D) nanorods, nanoribbons, quantum dots, etc., are receiving great attention toward it [5]. Especially 1D nanorods have excellent optoelectronic properties such as confinement of the charge carriers gets freely in 3-dimension. Also, it has a large surface-to-volume ratio of the 1D nanorods better charge collection, charge separation, and marginal recombination loss.

ZnS is the widely used semiconductor belonging to the II–VI system. It has been widely utilized in

LEDs, photodetectors, window layers, electroluminescence, etc. [6]. In addition to that Mg^{2+} doping into wurtzite, ZnS modifies the bandgap of pure ZnS, leading to an increase in optoelectronic properties [7]. The phase diagram of the solubility of Mg in ZnS at normal conditions is eutectic type. Approximately, 33 mol% doping of Mg in zincite was reported by a few authors [8]. Below the 4 mol%, ZnMgS unveil a stable wurtzite structure [9]. Another reason for facile Mg^{2+} doping in ZnS is the close ionic radius difference between Zn^{2+} 0.60 pm and Mg^{2+} 0.57 pm. Similarly, MgS is a stable material with a large bandgap; therefore, the Mg alloying in the ZnS increases the actual bandgap of pure ZnS. Also, Mg doping the zincite creates a lattice distortion because the electronegativity difference between Mg and Zn affects the electronic structure due to the Mg-3 s state, which dominates higher than the Zn-4 s state at the bottom of the conduction band. Thus it replicates in widening the bandgap energy, high dielectric constant, and high refractive index.

Mainly in the case of chemically synthesized ZnMgS/O thin films, large number of hydroxyl bonds are present on the surface layer and can easily break due to photon (light) exposure [10]. The broken H atom goes toward the interstitial position of ZnMgS/O and plays a role as a donor atom; therefore the resistivity of the ZnMgS decreases which results in the increment of efficiency. Due to such excellent characteristics properties, researchers are focusing on the synthesis, characterization, and optimization of stable ZnMgS, ZnMgO, MgO, MgS, etc. [11]. The alloy of the Mg-doped ZnS is synthesized by various physical and chemical techniques such as metal–organic chemical vapor deposition (MOCVD) [12], molecular beam epitaxy (MBE) [13], RF sputtering, and spray pyrolysis. But such physical synthesis techniques need sophisticated instruments and expert personnel to handle the same so it becomes costly. On the other hand, reports on the low-cost chemical synthesis of stable ZnMgS thin films are limited. For the first time on a glass substrate, A. S. Dive et al. reported the synthesis of $Zn_{0.8}Mg_{0.2}S$ 1D nanorod thin films using a low-cost one-step chemical bath deposition technique, which was explored to be used in visible light photosensors [14]. There are negligible reports available on the experiment, i.e., chemically synthesized and theoretical investigation of ZnMgS nanostructure. With this great motivation, in the present study, we have concentrated on low-cost chemical growth of the $Zn_{0.7}Mg_{0.3}S$ thin films on a commercial glass substrate and characterization of the films and made a scientific correlation of structural and optoelectronic properties of ZnMgS 1D nanorod thin films.

2 Experimental section

2.1 Synthesis of the $Zn_{0.7}Mg_{0.3}S$ thin films

Analytical reagent (AR) grade 98% pure chemicals were used for the synthesis of $Zn_{0.7}Mg_{0.3}S$ 1D nanorod thin films. In the chemical synthesis (CBD) procedure, an aqueous solution of zinc nitrate

hexahydrate [$Zn(NO_3)_2{\cdot}6H_2O$: 0.7 M], magnesium nitrate hexahydrate [$Mg(NO_3)_2{\cdot}6H_2O$: 0.3 M] and thiourea [H_2NCSNH_2: 0.1 M] were used. The detailed procedure was discussed in our previous report [15].

2.2 Characterization of the $Zn_{0.7}Mg_{0.3}S$ thin films

Bruker AXS, Germany (D8 Advanced) X-ray Diffractometer has been used for the exploration of structural chattels of the prepared $Zn_{0.7}Mg_{0.3}S$ 1D nanorod thin films. The scanning range of 20–60° (2θ) using $CuK\alpha_1$ radiation having a wavelength of 1.5406 Å with a scanning rate of 0.05 s^{-1} was used to record the XRD pattern. Field emission scanning electron microscopy (FE-SEM) assembled with energy dispersive X-ray analysis was carried out at instrument MIRA II LMH from TESCAN with an accelerating voltage of 5 and 30 kV. Tecnai G2 20 was used to carry out transmission electron microscopy (TEM) with selective area diffraction pattern (SEAD) with an accelerating voltage of 200 kV. Perkin-Elmer Lambda—25 UV–Vis spectrophotometer was used to measure the optical absorbance spectra in 300–1000 nm range. J–V characteristics were obtained from Keithley 2400 measurement setup in the presence of a class AAA solar simulator lamp as a light source.

2.3 Computational details

MedeA-(VASP) Vienna ab initio simulation package with the plane-wave pseudopotentials were used to calculate the detailed band structure, density of state (DOS), and total density of states (TDOS) of the ZnMgS. 2 × 2 × 2 supercells were built with the wurtzite ZnMgS unit cell with $P6_3mc$ as the space group. To investigate the effect of Mg doping in pure ZnS, three Mg atoms were substituted for Zn atoms to achieve a 30 mol% doping concentration. Other parameters such as residual force, minimum energy state, cut-off kinetic energy and smearing were kept similar as reported in our earlier publication [15, 16].

3 Result and discussion

3.1 XRD analysis

To investigate the structural properties of the nanocrystalline materials, X-ray diffraction (XRD) is an important characterization tool. Fig. 1 shows the XRD pattern of $Zn_{0.7}Mg_{0.3}S$ 1D nanorod thin films, which confirms the formation of the wurtzite hexagonal crystal structure matches with standard JCPDS # 37-1180 & # 36-1551. Also, the XRD pattern confirms that there is no other diffraction peak. The diffraction peaks were observed at 28.85° (111), 30.96° (101), 34.33° (002), 36.14° (101), 42.62° (200), 47.47° (102), and 56.25° (110) corresponding to the wurtzite hexagonal phase of the $Zn_{0.7}Mg_{0.3}S$ 1D nanorod thin films [17].

Fig. 1

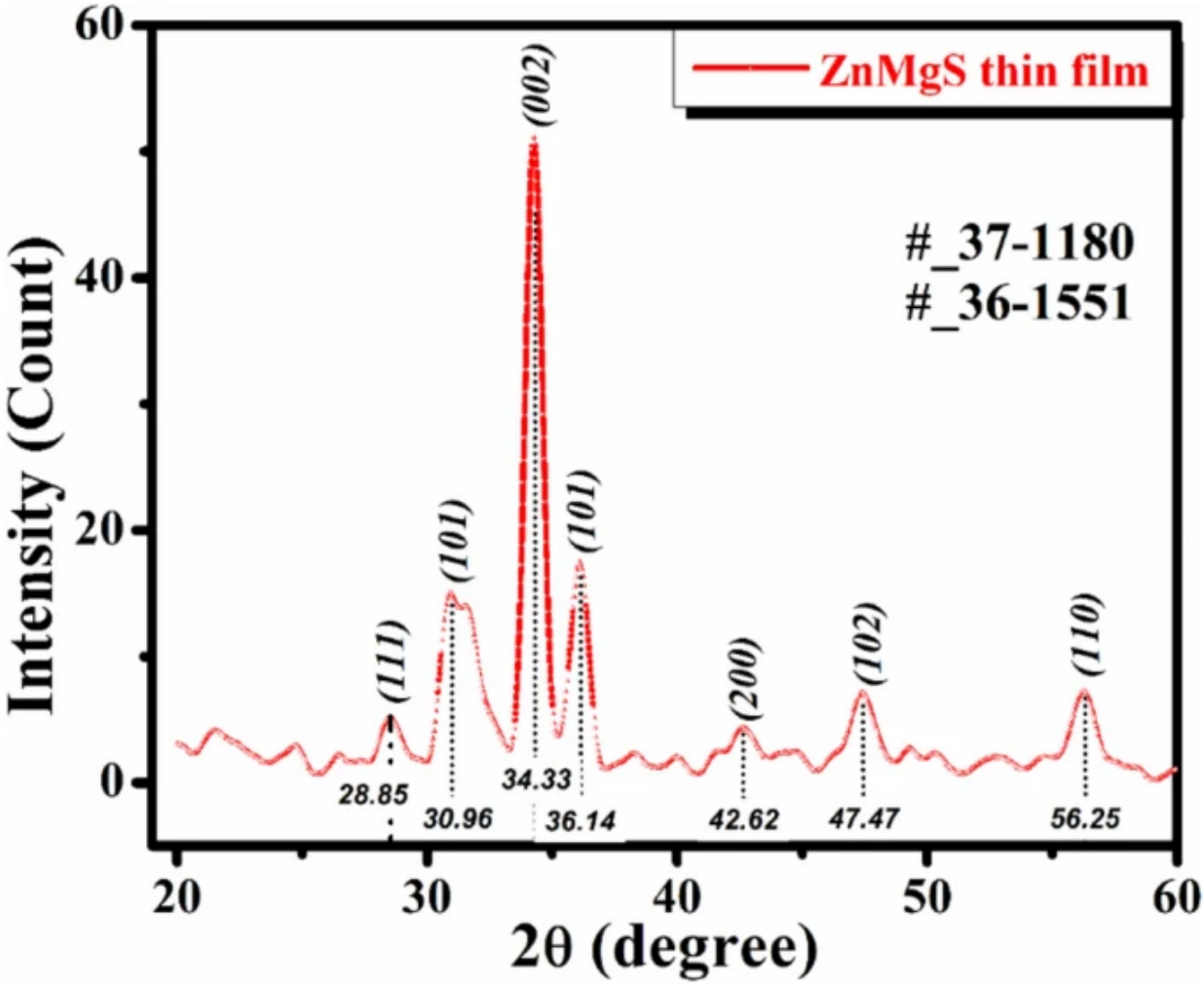

X-ray diffraction patterns of $Zn_{0.7}Mg_{0.3}S$ 1D nanorod thin films

The presence of a clear and highly intense diffraction peak at 34.33° (002) demonstrates that 1D nanorods are growing in a direction normal to the substrate's surface. [18]. Morphological studies also confirm the preferential growth toward the (002) direction of $Zn_{0.7}Mg_{0.3}S$ 1D nanorod thin films. It is reported earlier that, the pure ZnO has a multi-orientation growth with different shapes and structures, but in the case of Mg doping, most probable growth favored the c-axis [19, 20]. For calculating the lattice parameters and strain of the films, we used standard relations and strain equations, respectively. Also, the crystallite size was estimated using Scherrer's formula [14]. The calculated values are in good agreement with the previous reports available and listed in Table 1.

Table 1 Calculated structural parameters of $Zn_{0.7}Mg_{0.3}S$ 1D nanorod thin films estimated from XRD data

3.2 Morphological study

Figure 2a shows the typical FE-SEM micrographs of the $Zn_{0.7}Mg_{0.3}S$ 1D nanorod thin films synthesized onto the glass substrate. The magnified view is shown in Fig. 2b. The formation of a uniform layer of 1D nanorods can be observed clearly in FE-SEM micrographs, as well as in TEM micrographs and XRD diffraction results. Reducing the reflection losses due to the scattering of light is the main characteristic of the nanorod morphology and can help to increase the light-trapping efficiency marginally. Therefore, as compared to other nanocrystalline geometries, 1D nanorods provide a better interfacial area and give an upsurge in the carrier concentration. So such type of nanostructure can conceivably give better efficiency in the nanostructured photonic devices [19]. Figure. 2c shows that the EDAX spectrum of the $Zn_{0.7}Mg_{0.3}S$ 1D nanorod thin films confirms the compositional ratio of the Zn, Mg, S, and O, respectively. The atomic ratio of the Zn, Mg, S and O which confirmed from the EDAX spectrum was to be 40:20:30:10 which is most reliable with a stoichiometry of $Zn_{0.7}Mg_{0.3}S$ composition [15]. Due to open-air reactions and deionized (DI) water used in the reaction as solvent, almost 9–10% of oxide were found in the EDAX spectra. Additional structural studies regarding the crystallinity and particle size of the as-prepared $Zn_{0.7}Mg_{0.3}S$ 1D nanorod thin films were analyzed by transmission electron microscopy (TEM) micrographs. Fig. 2d, e shows the TEM micrographs inset with the selected area diffraction pattern (SAED). The average length and diameter of the as-prepared nanorods were approximately ~ 180 nm and ~ 4 μm, respectively [15]. The particle size calculated from the TEM images was ~ 29 nm which was in good agreement with XRD results. The discrete spot pattern in the SAED pattern is the characteristic evidence of the formation of 1D nanorods toward the (002) plane. The SAED pattern also confirms the formation of stable wurtzite hexagonal structure formation of $Zn_{0.7}Mg_{0.3}S$ 1D nanorod thin films.

Fig. 2

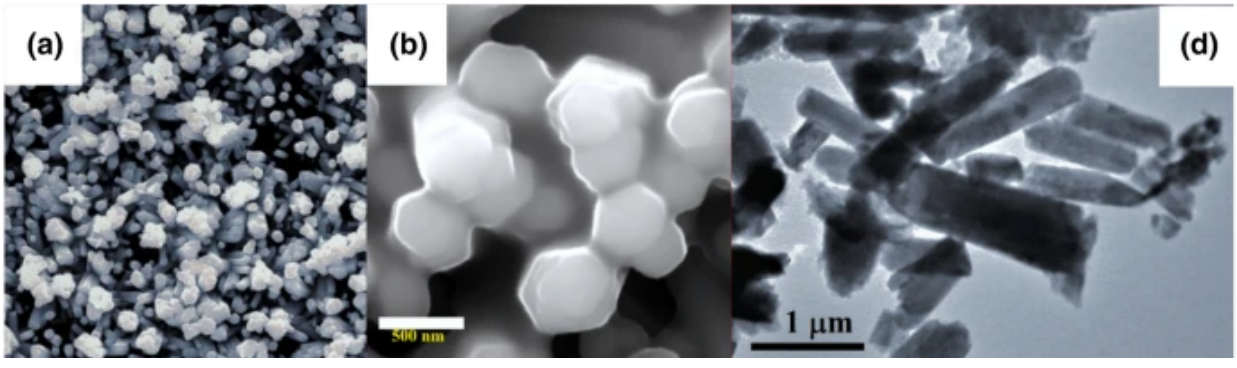

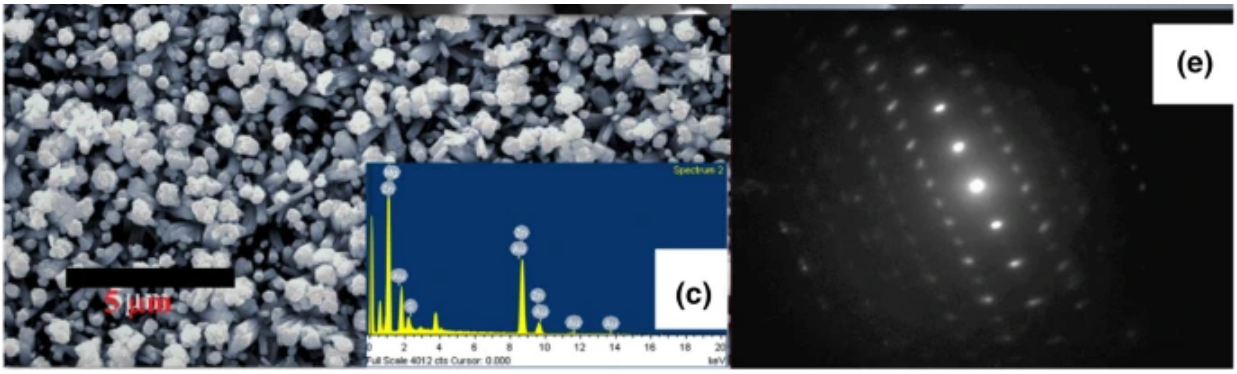

a FE-SEM micrograph of thin film, **b** inset magnified view of nanorods, **c** EDAX spectra of NR thin film, and **d** TEM micrograph of thin film **e** SAED pattern

3.3 Optical analysis

3.3.1 UV–Vis absorbance study and photoluminescence spectroscopy

Because 1D nanostructures like nanowires and nanorods have the potential ability to increase light trapping at the device, they may attract a lot of interest. The UV–Vis absorbance spectra as a function of wavelength, Tauc's plot for the bandgap determination, and photoluminescence (PL) spectra for the $Zn_{0.7}Mg_{0.3}S$ 1D nanorod thin films are represented in Fig. 3a, b and c, respectively. It can be see that ZnMgS films show the blue shift ~ 380 nm [20]. The Moss-Burstein effect occurs after the addition of Mg in Zn alloys which enhances the bandgap values [21].

Fig. 3

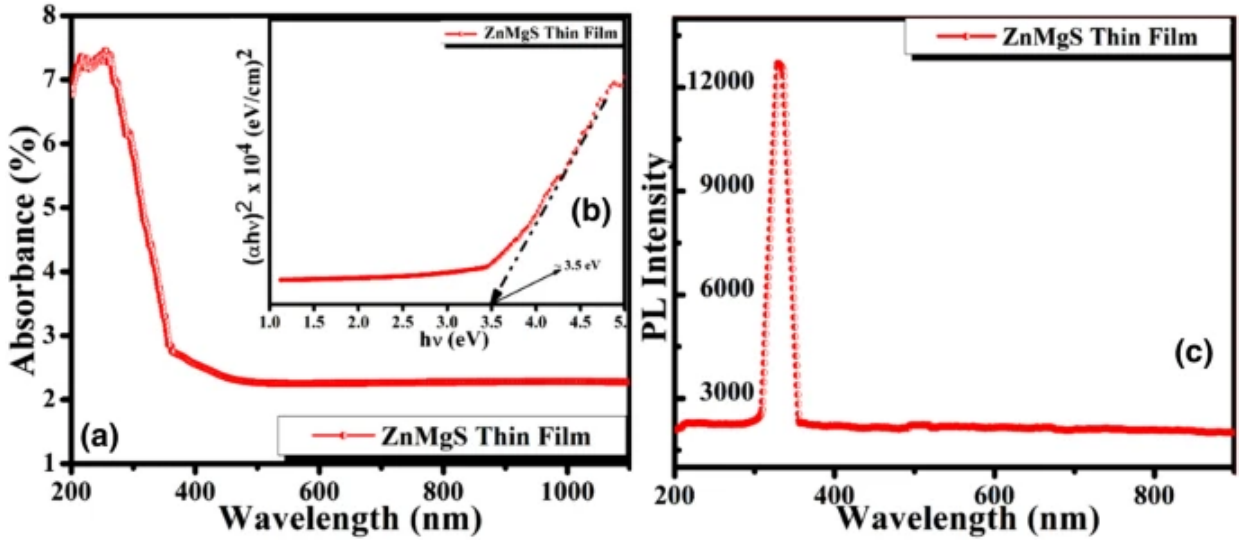

a UV–Vis absorbance spectra ZnMgS thin film, **b** inset Tauc's pot and **c** photoluminescence spectrum of ZnMgS thin film

Also, one of the interesting modifications that have been seen after the incorporation of Mg^{2+} in Zn^{2+} alloys is an increase in oxygen vacancies as well as electron concentration. Some new electronic states have occurred in the conduction band (CB) and valance band (VB) with an additional heightening of CB. Therefore, such electronically modified materials play a major role in the absorption & reaching of extra light to the device. The findings are consistent with prior reports based on the experimental and theoretical investigation. The PL spectroscopy is the most useful characterization tool to investigate the emission, vacancies, and defects in doped and undoped ZnO and ZnS structures. The substantial excitation peak at ~ 370 nm is seen in Fig. 3c which indicates UV emission by recombination of free excitons [22, 23]. The doping of Mg^{2+} in the actual structure of ZnS will enhance the bandgap values which was confirmed in the UV–Vis absorption study and electronic structure optimization results can be correlated here.

3.3.2 Raman spectrum analysis

To analyze the crystal structure, lattice distortion, defect-induced disorder, and modification that occurred after the doping or post-deposition treatment, an important tool Raman study was performed The chemically synthesized $Zn_{0.7}Mg_{0.3}S$ 1D nanorod thin films belong to a hexagonal wurtzite structure with a $P6_3mc$ space group. The group theory has predicted that the optical phonon modes can be classified via irreducible representation [14]. Both A_1 and E_1 modes are split into transverse optic (TO) and longitudinal optic (LO) modes, respectively. Additionally, E_2 has two different modes as E_2

(high) and E_2 (low) which represent the motion of Zn sublattice and motion of the oxygen vacancies, respectively [14]. Fig 4 represents the room temperature Raman spectra of the $Zn_{0.7}Mg_{0.3}S$ 1D nanorod thin films. The peak E_2 (high) optical phenomenon at 440 cm^{-1} is the characteristic of the wurtzite hexagonal phase of the ZnMgS/O which is also confirmed by the XRD analysis [24]. Another peak present at 475 cm^{-1} belonging to LO mode is the evidence of the growth of stable phase ZnMgS thin films [25].

Fig. 4

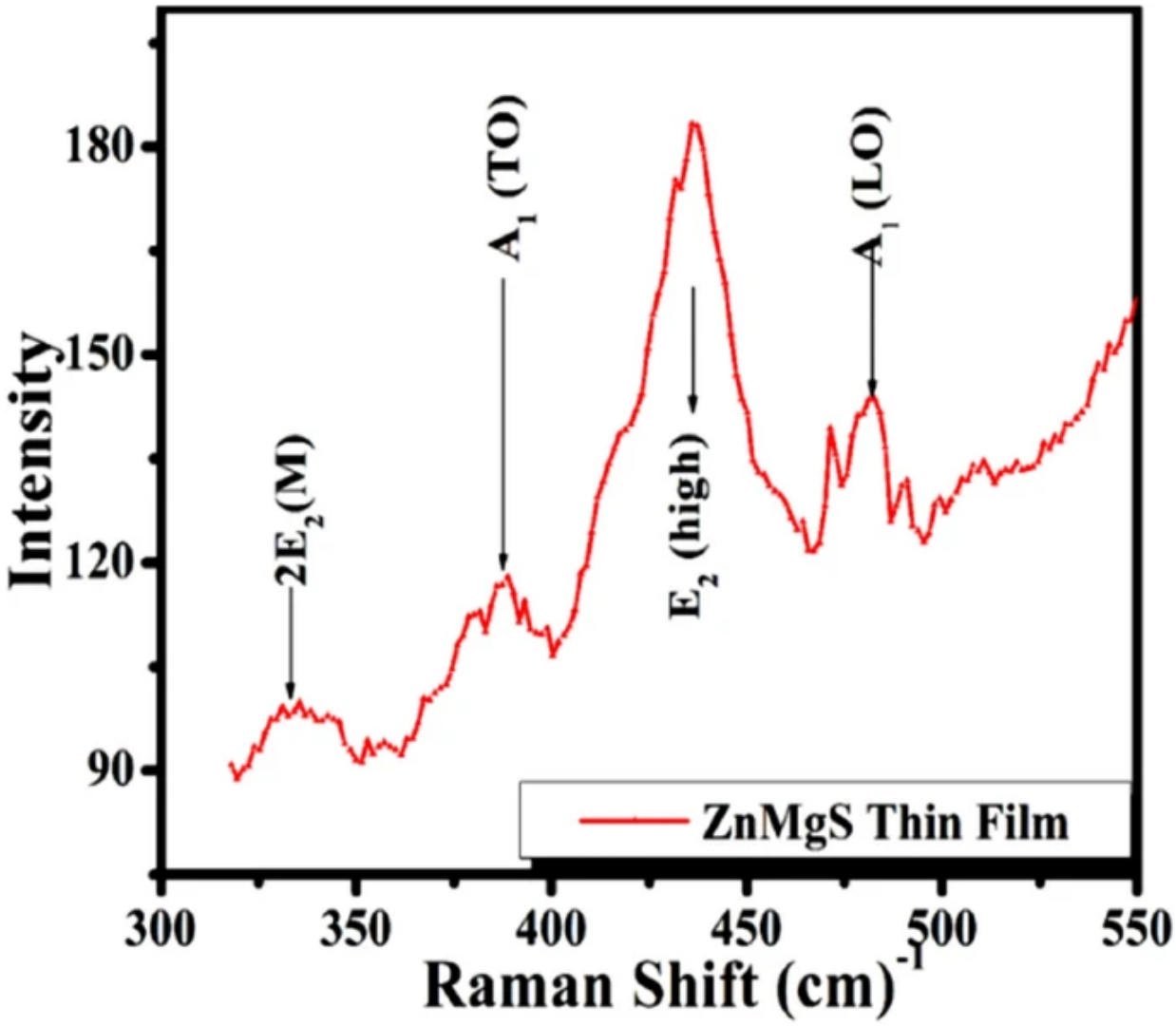

Raman spectra of $Zn_{0.7}Mg_{0.3}S$ 1D nanorod thin films

Also, the peaks at 500 cm^{-1} and 540 cm^{-1} may be due to structural imperfections, oxygen vacancies, and Zn interstitials. The second-order Raman scattering was seen from 324 to 400 cm^{-1} which was

recognized as transverse acoustic + longitudinal optical (TA + LO) phonon modes at 335 cm^{-1} and 385 cm^{-1} for the $Zn_{0.7}Mg_{0.3}S$ 1D nanorod thin films.

3.3.3 J–V Characteristics study

To investigate the charge transportation properties of the as-prepared $Zn_{0.7}Mg_{0.3}S$ 1D nanorod thin films, we have measured the current density vs voltage (J–V) characteristics. The J–V measurement has done at room temperature in dark and illumination conditions. The illumination intensity was kept at ~ 100 W/cm^2 and the applied bias voltage was ± 5 V. Figure 5 shows the typical J–V plot of $Zn_{0.7}Mg_{0.3}S$ 1D nanorod thin film and the measurement was done on 1 × 1 cm film. To make proper electrical contacts between film and connecting pins, the silver (Ag) paste was used. Ohmic behavior has been verified based on the J–V plot since the generated current is proportionate to the applied voltage. After applying photonic illumination (100 W/cm^2) to the film, a significant change occurred in current values which is the confirmation of the generation of large no. of free electron–hole pairs in the conduction and valance band. Moreover, the energy of incident photons can easily break the covalent bonds which result in the increment of the charge carrier concentration at both valance and conduction bands. The value of the resistance calculated by the J–V plot was 1.43×10^6 Ω for dark and 1.12×10^4 Ω for illumination conditions [26]. The calculated photosensitivity (S) and photoresponsivity (R) with the help of standard relation were found to be ~ 98% and ~ 37.6 μA/W, respectively [14, 27]. Also, the photocurrent for $Zn_{0.7}Mg_{0.3}S$ 1D nanorod thin film was found to be 0.41 mA; this is marginally greater compared to the previous reports on photosensing of ZnO, ZnS, etc. As well, the increased photoresponse of ZnMgS films may be due to the better charge transformation amid the device after the doping of Mg. Therefore such materials draw great attention due to their uses in solar cell window layers and other optoelectronic devices.

Fig. 5

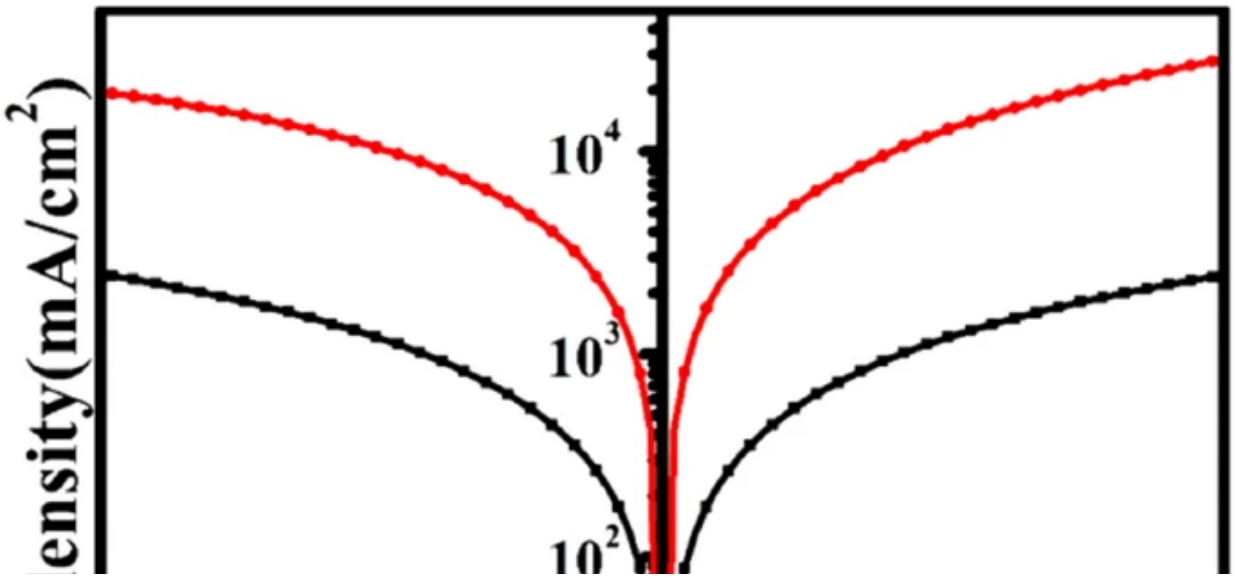

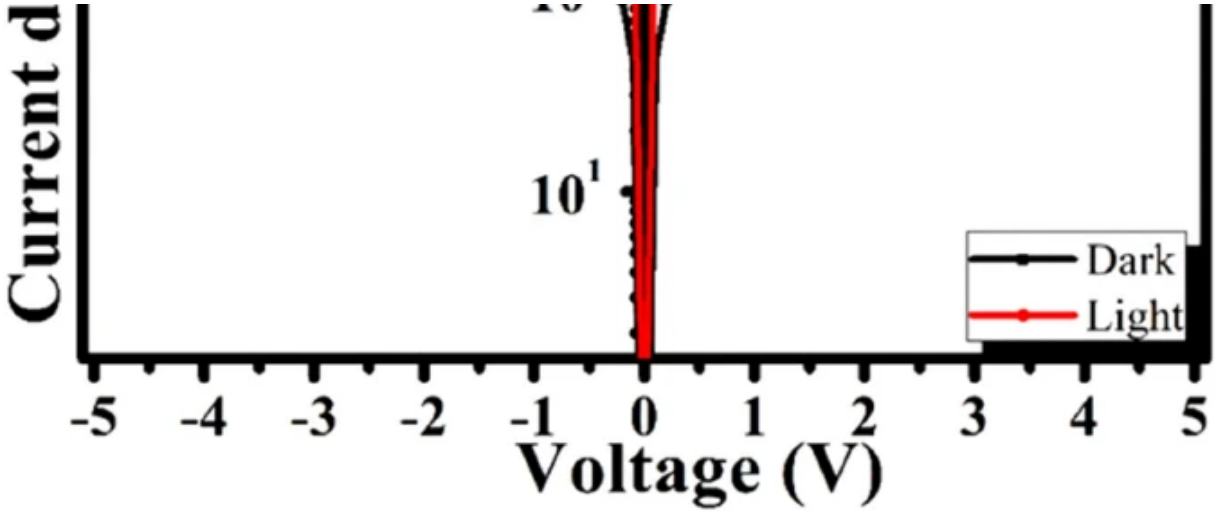

J–V plot of the $Zn_{0.7}Mg_{0.3}S$ 1D NR thin film for dark and light

3.3.4 Electronic structure investigation

The effect of doping of magnesium (Mg) on the electronic structure of pure ZnS nanocrystals was investigated via first-principle calculations in which theoretical bandgap, total, summed and partial density of states (DOS) have been simulated by using Generalized Gradient Approximation (GGA) of the DFT. Initially, the structural optimization of the ZnS and Mg-doped ZnS was performed successfully. The optimized lattice parameters for the pure and $Zn_{0.7}Mg_{0.3}S$ structure were a = 3.83 Å, c = 5.35 Å and a = 3.84 Å, c = 5.32 Å. The theoretical band structure plot of the optimized ZnMgS structure reveals the direct bandgap semiconductor with an energy bandgap of 1.55 eV as shown in Fig. 6f. The conduction band minima and valance band maxima of the calculated wurtzite structure were located at the "Γ" point of the first Brillion zone which is the confirmation of direct bandgap and can be seen in Fig. 6a, b, c, d, e and f. The same results were also confirmed from the optical and electrical study of the ZnMgS films. Other than the wurtzite hexagonal structure, few reports were available on the rock salt-structured ZnMgS having an indirect bandgap. The indirect bandgap materials are having a phonon addition between electron and photon which results from the optical inactiveness [28, 29]. Consequently, such direct bandgap semiconductor materials state their dominance in optoelectronics technology. Also, the bandgap value and lattice parameters estimated from the theoretical calculation were comparable to previous results. Table 2 shows the comparative analysis of the various parameters obtained from the DFT calculations. It is a well-known problem reported in theoretical study that, the misinterpretation of the band dispersion occurs in localized density approximation (LDA) and GGA calculations located at the Zn-3d band erroneously. Such Zn-3d follows the top of the valance band and creates strong hybridization between O-2p which makes the remarkable reduction in bandgap energy theoretically likened to experimental values [30, 31].

Fig. 6

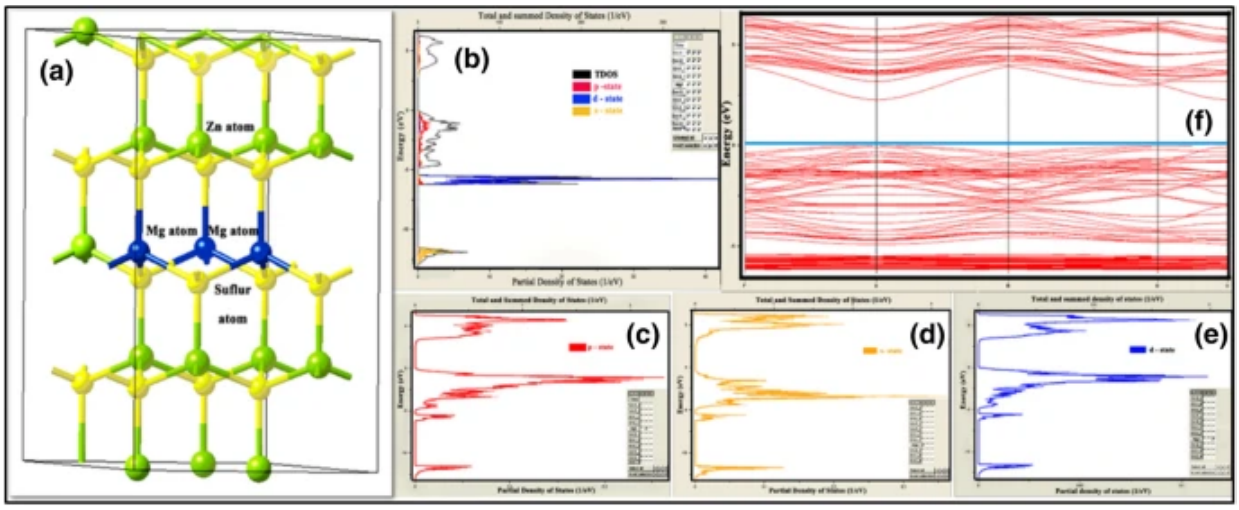

a Optimized unit cell of ZnMgS, **b** calculated density of states of ZnMgS, **c**– **e** focused view of p state, s state and d state and **f** calculated band structure of ZnMgS

Table 2 Comparison of various parameters obtained from DFT calculation with similar structure and application

4 Conclusion

$Zn_{0.7}Mg_{0.3}S$ 1D nanorod thin films were successfully synthesized by the chemical technique on a glass substrate with a short deposition time. Such chemical technique is simple, cheaper, and easy to handle; hence, we have utilized it. The first-principle investigation of ZnMgS has been carried out by MedeA-(VASP) DFT simulation package. The theoretical results were correlated with experimental outcomes and the ZnMgS shows the direct bandgap semiconducting behavior. The structural analysis of $Zn_{0.7}Mg_{0.3}S$ showed good crystallinity with ~ 24 nm by XRD and ~ 29 nm from the SAED pattern. Stoichiometry of the films was studied and confirmed by the EDAX spectra. Vertically aligned nanorods have been seen on the surface of the substrate by FE-SEM micrographs. The optical absorbance studies showed the maximum absorbance in the UV region (~ 380 nm) and an energy gap of ~ 3.5 eV. The J–V characteristics plot of ZnMgS shows the potential increase in the photocurrent (~ 37.6 μA/W) when it was illuminated by a 100 W solar simulator lamp. These inexpensive semiconductors were demonstrated to be suitable for use in future optical devices by the optoelectronic features that were

investigated here.

Data availability

Dr. Babasaheb Ambedkar Marathwada University, Aurangabad, UGC-DAE CSR Indore and IUAC, New Delhi.

References

1. I.A. Buyanova, W.M. Chen, M.P. Ivill, R. Pate, D.P. Norton, S.J. Pearton, J.W. Dong, A. Osinsky, B. Hertog, A.M. Dabiran, P.P. Chow, Optical characterization of ZnMnO-based dilute magnetic semiconductor structures. J. Vac. Sci. Technol. **24**, 259–262 (2006)

Article CAS Google Scholar

2. M.A. Pietrzyk, M. Stachowicz, D. Jarosz, R. Minikayev, M. Zielinski, P. Dluzewski, A. Kozanecki, Properties of ZnO/ZnMgO nanostructures grown on r-plane Al2O3 substrates by molecular beam epitaxy. J. Alloy. Compd. **650**, 256–261 (2015)

Article CAS Google Scholar

3. H. Wang, H. Long, Z. Chen, X. Mo, S. Li, Z. Zhong, G. Fang, Fabrication and characterization of alternating-current-driven ZnO-based ultraviolet light-emitting diodes. Electron. Mater. Lett. **11**, 664–669 (2015)

Article CAS Google Scholar

4. M.-M. Fan, K.-W. Liu, X. Chen, Z.-Z. Zhang, B.-H. Li, H.-F. Zhao, D.-Z. Shen, Realization of cubic ZnMgO photodetectors for UVB applications. J. Mater. Chem. C **3**, 313–317 (2015)

Article CAS Google Scholar

5. H.J. Fan, Y. Yang, M. Zacharias, ZnO-based ternary compound nanotubes and nanowires. J. Mater. Chem. **19**, 885–900 (2009)

Article CAS Google Scholar

6. E. Omurzak, T. Mashimo, S. Sulaimankulova, S. Takebe, L. Chen, Z. Abdullaeva, C. Iwamoto, Y. Oishi, H. Ihara, H. Okudera, A. Yoshiasa, Wurtzite-type ZnS nanoparticles by pulsed electric discharge. Nanotechnology (2011). https://doi.org/10.1088/0957-4484/22/36/365602

Article Google Scholar

7. K. Ichino, K. Ueyama, M. Yamamoto, H. Kariya, H. Miyata, H. Misasa, M. Kitagawa, H. Kobayashi, High temperature growth of ZnS and ZnMgS by molecular beam epitaxy under high sulfur beam pressure. J. Appl. Phys. **87**, 4249–4253 (2000)

Article CAS Google Scholar

8. T. Mashimo, E. Omurzak, L. Chen, R. Inoue, C. Kawai, Effect of shock compression on wurtzite-type ZnMgS crystals. J. Appl. Phys. **10**(1063/1), 3532045 (2011)

Google Scholar

9. I. Khan, I. Ahmad, H.A.R. Aliabad, M. Maqbool, Effect of phase transition on the optoelectronic properties of Zn1-xMgxS. J. Appl. Phys. **10**(1063/1), 4756040 (2012)

Google Scholar

10. S. Kim, C.-S. Lee, S. Kim, R.B.V. Chalapathy, E.A. Al-Ammar, B.T. Ahn, Understanding the light soaking effect of ZnMgO buffer in CIGS solar cells. Phys. Chem. Chem. Phys. **17**, 19222–19229 (2015)

Article CAS Google Scholar

11. K.A. Prior, C. Bradford, I.A. Davidson, R.T. Moug, Metastable II-VI sulphides: growth, characterization and stability. J. Cryst. Growth **323**, 114–121 (2011)

Article CAS Google Scholar

12. A. Toda, T. Asano, K. Funato, F. Nakamura, Y. Mori, Epitaxial growth of ZnMgSSe on GaAs substrate by metalorganic chemical vapor deposition. J. Cryst. Growth **145**, 537–540 (1994)

Article CAS Google Scholar

13. C. Morhain, X. Tang, M. Teisseire-Doninelli, B. Lo, M. Laugt, J.M. Chauveau, B. Vinter, O. Tottereau, P. Vennegues, C. Deparis, G. Neu, Structural and electronic properties of ZnMgO/ZnO quantum wells. Superlattices Microstruct. **38**, 455–463 (2005)

Article CAS Google Scholar

14. A.S. Dive, N.P. Huse, K.P. Gattu, R. Sharma, Soft chemical growth of Zn 0.8 Mg 0.2 S one dimensional nanorod thin films for efficient visible light photosensor. Sens Actuators A **266**, 36–45 (2017)

Article CAS Google Scholar

15. A.S. Dive, K.P. Gattu, N.P. Huse, D.R. Upadhayay, D.M. Phase, R.B. Sharma, Single step chemical growth of ZnMgS nanorod thin film and its DFT study. Mater. Sci. Eng. **228**, 91–95 (2018)

Article CAS Google Scholar

16. A.S. Dive, N.P. Huse, K.P. Gattu, R.B. Birajdar, D.R. Upadhyay, R. Sharma, Theoretical and experimental investigations of intermediate bands in ZnS–Mg nanocrystalline thin film photosensor. J. Mater. Sci. (2017). https://doi.org/10.1007/s10854-017-7393-5

Article Google Scholar

17. A. Dive, N. Huse, D. Upadhye, S. Bagul, K. Gattu, R. Sharma, Growth of nanocrystalline $Zn_{0.75}Mg_{0.25}S$ thin film by solution growth technique and their characterization as a window layer for solar cell. Ferroelectrics **518**, 1–8 (2017)

Article CAS Google Scholar

18. L. Meng, J. Zhang, Q. Li, X. Hou, Enhancement of two-dimensional electron-gas properties by Zn polar ZnMgO/MgO/ZnO structure grown by radical-source laser molecular beam epitaxy. J.

Nanomater. (2015). https://doi.org/10.1155/2015/694234

Article Google Scholar

19. A. Rivera, A. Mazady, M. Anwar, Co-axial core-shell ZnMgO/ZnO NWs. Solid-State Electron **104**, 126–130 (2015)

Article CAS Google Scholar

20. M.A. Pietrzyk, M. Stachowicz, A. Wierzbicka, A. Reszka, E. Przezdziecka, A. Kozanecki, Properties of ZnO single quantum wells in ZnMgO nanocolumns grown on Si (111). Opt. Mater. **42**, 406–410 (2015)

Article CAS Google Scholar

21. A. Santhamoorthy, P. Srinivasan, A. Krishnakumar, J.B.B. Rayappan, K.J. Babu, SILAR-deposited nanostructured ZnO thin films: effect of deposition cycles on surface properties. Bull. Mater. Sci. **44**, 1–8 (2021)

Article CAS Google Scholar

22. K. Ichino, N. Suzuki, H. Kariya, K. Ueyama, M. Kitagawa, H. Kobayashi, Optical properties of ZnS/ZnMgS strained-layer quantum wells. J. Cryst. Growth **214**, 368–372 (2000)

Article Google Scholar

23. A.S. Dive, N.P. Huse, K.P. Gattu, R. Sharma, A high visible light ZnMgS nanorod thin film photosensor by solution growth technique. AIP Conf. Proc. **1832**, 120007 (2017)

Article CAS Google Scholar

24. M.A. Akram, S. Javed, M. Islam, M. Mujahid, A. Safdar, Arrays of CZTS sensitized ZnO/ZnS and ZnO/ZnSe core/shell nanorods for liquid junction nanowire solar cells. Sol. Energy Mater. Sol. Cells **146**, 121–128 (2016)

Article CAS Google Scholar

25. D.H. Wang, D.M. Huang, C.X. Jin, X.H. Liu, Z. Lin, J. Wang, X. Wang, Raman spectra of Zn1-xMgxSySe1-y quaternary alloys. J. Appl. Phys. **80**, 1248–1250 (1996)

Article CAS Google Scholar

26. N.P. Huse, A.S. Dive, K.P. Gattu, R. Sharma, An experimental and theoretical study on soft chemically grown CuS thin film for photosensor application. Mater. Sci. Semicond. Process. **67**, 62–68 (2017)

Article CAS Google Scholar

27. N.P. Huse, A.S. Dive, K.P. Gattu, R. Sharma, One step synthesis of kestarite Cu_2ZnSnS_4 thin film by simple and economic chemical bath deposition method. AIP Conf. Proc. **1832**, 080082 (2017)

Article CAS Google Scholar

28. A. Djelal, K. Chaibi, N. Tari, K. Zitouni, A. Kadri, Ab-initio DFT-FP-LAPW/TB_mBJ/LDA-GGA investigation of structural and electronic properties of Mg x Zn 1−x O alloys in würtzite rocksalt and zinc-blende phases. Superlattices Microstruct (2017). https://doi.org/10.1016/j.spmi.2017.04.041

Article Google Scholar

29. I.A. Imad Khan, H.A. Rahnamaye Aliabad, M. Maqbool, Effect of phase transition on the optoelectronic properties of Zn1-xMgxS. J. Appl. Phys. **112**, 0731041–0731046 (2012)

Google Scholar

30. F.C. Zhang, H.W. Cui, X.X. Ruan, W.H. Zhang, Study on Density Functional Theory of $Zn_{1-x}Mg_xO$ Alloy. Appl. Mech. Mater. **556–562**, 177–180 (2014)

Google Scholar

31. C. Feigl, S.P. Russo, A.S. Barnard, A comparative density functional theory investigation of the mechanical and energetic properties of ZnS. Mol. Simul. **37**, 321–333 (2011)

Article CAS Google Scholar

32. H. Lashgari, A. Boochani, A. Shekaari, S. Solaymani, E. Sartipi, R.T. Mendi, Electronic and optical properties of 2D graphene-like ZnS: DFT calculations. Appl. Surf. Sci. **369**, 76–81 (2016)

Article CAS Google Scholar

33. A.Z.M. Dadsetani, First principle investigations of the optical properties of Zn1-xMgxS, Zn1-xMgxSe and Zn1-xMgxTe ternary alloys. Int. J. Mod. Phys. B **28**, 1450211–14502119 (2014)

Article CAS Google Scholar

34. M.Y. Shahid, M. Asghar, H.M. Arbi, M. Zafar, S.Z. Ilyas, Role of magnesium in ZnS structure: Experimental and theoretical investigation. AIP Adv. **6**, 025019 (2016)

Article CAS Google Scholar

Funding

Not applicable.

Author information

Authors and Affiliations

Department of Physics, Shri. Dr. R. G. Rathod Arts & Science College, Dist. Akola, Murtizapur, MS, 444107, India

Avinash S. Dive

Department of Physics, Late R. B. Arts, Commerce and Smt. S. R. B. Science College, Dist. Yavatmal,

Arni, MS, 445103, India
Jitendra S. Kounsalye

Department of Physics, Dr. Babasaheb Ambedkar Marathwada University, Aurangabad, MS, 431004, India
Ramphal Sharma

Contributions

The author ASD synthesized the thin films, characterized them and performed the theoretical calculation, JSK helped to analyze and writing of structural and optical results. RS guided for overall work and writing of DFT results.

Corresponding author

Correspondence to Avinash S. Dive.

Ethics declarations

Conflict of interest

The authors declare that they have no competing interest.

Ethical approval

Not applicable.

Consent to participate

Not applicable.

Consent to publish

Not applicable.

Additional information

Publisher's Note

Rights and permissions

About this article

Cite this article

Dive, A.S., Kounsalye, J.S. & Sharma, R. Growth, structural, morphological, opto-electrical and first-principle investigations of ZnMgS thin films. *J Mater Sci: Mater Electron* **33**, 18798–18806 (2022). https://doi.org/10.1007/s10854-022-08729-1

Received	Accepted	Published
01 May 2022	05 July 2022	16 July 2022

Issue Date
August 2022

DOI
https://doi.org/10.1007/s10854-022-08729-1

Share this article